Alternative small-scale tests to characterize the structural behaviour of steel fibre-reinforced sprayed concrete

Alternative small-scale tests to characterize the structural behaviour of steel fibre-reinforced sprayed concrete

Alan Renato Estrada Cáceres[1*], Sergio H. P. Cavalaro[2], Renata Monte[3], Antonio Domingues de Figueiredo[4]

1. *Dept. of Civil Construction Engineering, Polytechnic School, University of São Paulo, Caixa Postal 61548. CEP 05508-900, Sao Paulo, Brazil, alan.estrada@usp.br.*
2. *School of Architecture, Building and Civil Engineering, Loughborough University, Loughborough, Leics, LE113TU, UK, S.Cavalaro@lboro.ac.uk.*
3. *Dept. of Civil Construction Engineering, Polytechnic School, University of São Paulo, Caixa Postal 61548. CEP 05508-900, Sao Paulo, Brazil, renata.monte@usp.br.*
4. *Dept. of Civil Construction Engineering, Polytechnic School, University of São Paulo, Caixa Postal 61548. CEP 05508-900, Sao Paulo, Brazil, antonio.figueiredo@usp.br.*

* Corresponding author. Tel.: +55 (11) 3091-5165; fax: +55 (11) 3091-5544;
E-mail: alan.estrada@usp.br

Abstract

The flexural beam test EN 14488-3 is considered a reference for the characterization of the post-cracking tensile response of fibre-reinforced sprayed concrete (FRSC). However, the geometry of the specimens is a complication in case of characterising specimens extracted from the structure. The double punch test (DPT) and double-edge wedge splitting (DEWS) test are two alternative approaches that have been introduced to simplify the assessment of the post-cracking response of fibre reinforced-concrete. These tests could allow the characterisation of samples extracted from sprayed test panels or even existing structures. The objective of this experimental study is to demonstrate the possibility to correlate the flexural beam test EN 14488-3, the DPT and DEWS tests, and verify the capacity of these tests in predicting the constitutive model of FRSC. The results indicated high correlations (R^2 above 0.98) between tests. The constitutive models obtained from the alternative tests were close to those determined employing the flexural beam test. Both the DPT and DEWS test can replace the EN 14488-3 test in systematic quality control or for the confirmation of design parameters of FRSC structure. However, the DEWS test requires more time to prepare the specimens, being more appropriate to parameterize the constitutive models of the FRSC. The DPT, due to its simplicity of execution, becomes more practical for quality control of FRSC. Specimen with different size subjected to the DPT show a similar residual strength pattern.

***Keywords**: Sprayed concrete, fibre-reinforced concrete, flexural beam test, DPT test, DEWS test.*

1. Introduction

One of the most common methods to characterize fibre-reinforced sprayed concrete (FRSC) is the four-point flexural beam test EN 14488-3 (Bernard; Thomas, 2020). Initially, this test was proposed by EFNARC (1996) and now is detailed in the standard EN 14488-3: 2004 (AENOR, 2004). Recent guidelines such as those of ITA Working Group No. 12 and ITAtech (ITA, 2020) propose the three-

point flexural test on a beam with a notch EN 14651 to obtain design parameters for FRSC structures according to the provisions in the *fib* Model Code. This reflects the current aspiration of adopting the design philosophy of fibre-reinforced concrete (FRC) structures in sprayed concrete structures (Larive *et al*. 2020). However, due to the production process of FRSC elements, tests performed in beams need to be extracted from sprayed test panels. This implies a laborious cutting process and difficulties in handling heavy panels. Spraying process factors such as the effect of the spray direction (Figueiredo, 1997; Jolin, 1999; Kaufmann *et al*. 2013) and rebound (Figueiredo, 1997; Austin; Peaston; Robins, 1997; Armelin, 1997; Jolin, 1999; Kaufmann *et al*. 2013; Ginouse; Jolin, 2016) produce a significant variation in fibre content and orientation in the tunnel lining if compared with equivalent sprayed specimens.

Studies show high variability of results of the flexural characterization of FRSC beams in a range of 20 to 30% (Morgan; Mindess; Chen, 1995; Bernard, 2002; Juhasz; Nagy; Shaul, 2017; Galobardes *et al*., 2019; Hanke *et al*., 2001 *apud* Bernard; Thomas, 2020). This phenomenon has been attributed to the small fracture surface of the specimen, which is prone to significant variation in the content and orientation of fibres crossing the cracked surface (Tran; Bernard; Beasley, 2005; Bernard, 2013; Carmona; Molins, 2019; Galobardes *et al*., 2019). The uncertainty of results can also be exacerbated by the post-peak instability caused by the abrupt transfer of load from the matrix to the fibres during cracking (Nguyen, 2003; Bernard, 2013). To lessen the effect of post-peak instability, flexural beam tests require high-quality testing machines with a closed-loop system (EN 14488-3, 2004; Bernard, 2009) that are not available in most technological control laboratories in Latin America (Silva, 2017), for example.

Other tests were developed to evaluate FRC, such as the double punching test (DPT), also known as Barcelona and double-edge wedge splitting test (DEWS). These tests procedures have the advantage of using smaller specimens, which can simplify the systematic quality control evaluation of existing FRSC structures through extracted samples or can be used for confirmation of design parameters. The common criteria considered when selecting the most appropriate test to evaluate structures are the reliability of the results, the cost of the tests and whether the sample is representative of the in-situ concrete (Nguyen, 2003). Smaller-scale tests allow the evaluation of a larger number of samples, enabling a broader and more robust analysis of data (Galobardes; Figueiredo, 2015), especially when it is desired to evaluate the behaviour of the material in FRSC structures that have great variability.

The DPT is supported by a large body of research and has been increasingly used for the quality control of FRC in real projects (Carmona; Aguado; Molins, 2013; Blanco *et al*., 2014; Monte *et al*., 2016; Galeote *et al*., 2017; Carmona; Molins; Aguado, 2018; Rambo *et al*., 2018; Segura-Castillo *et al*., 2018; Carmona and Molins, 2019; Simão *et al*., 2019; Nogueira *et al*. 2020). Three cracks form during the test due to the internal stresses induced by cylinder punches located on the top and bottom of the specimens. The cracks usually evolve following a mix of types I and II fracture mode, which differs from the cracks in the bending test of beams that tend to display a type I fracture (Galeote *et al*., 2017).

The DEWS test developed by Di Prisco; Ferrara; Lamperti (2013) is also an indirect tensile test. Wedges placed in notches on two opposite faces of the specimen produce internal tensile forces that lead to crack formation and opening. The setup aims to create an approximately uniaxial tensile stress over the cross-section of the specimen, leading to a type I fracture mode. Di Prisco; Ferrara; Lamperti (2013) recommend the use of six LVDTs (linear variable displacement transducers) and a very slow loading speed (displacement rate of 0.012 mm/min). Borges *et al*. (2019) proposed a simplified variation of the test with 10 times higher loading speed and only 2 extensometers, one at the centre of each face of the specimen to measure the crack-opening, providing greater dynamism to the method, reducing the time and execution work.

Few studies have evaluated FRSC using the DPT. Silva (2017) evaluated the scatter of load results from the DPT, statistically proving that there is no significant difference in results of specimens extracted from different panels. Segura-Castillo *et al*. (2018) studied the anisotropy in the tensile response of FRSC through the DPT and inductive test. Galobardes *et al*. (2019) correlated the DPT using cylinders with a height and diameter of 100 mm with the flexural beam test EN 14488-3, obtaining a good correlation (R^2 = 0.97) between the residual strength of both tests. Using the same cylinder size, Monteiro and Silva (2020) evaluated the influence of the machine stiffness on the DPT and correlated the results with those of the EN 14651 test, finding good correlations in terms of residual strength (mean R^2 0.96). The influence of the size of the cylindrical core of the DPT on the correlation of results with the EN 14488-3 test was not evaluated. To the authors' best knowledge, no study has applied the DEWS test to characterise FRSC recently. Consequently, no study has compared the post-cracking behaviour obtained with DPT, DEWS and the flexural bending tests in FRSC specimens or the constitutive models calculated from these test results in FRSC.

The objective of this study is to demonstrate the possibility to correlate the residual strength results of the flexural beam test EN 14488-3 with those of the DPT (in cylinders with 2 sizes) and DEWS test, in the evaluation of steel fibre-reinforced sprayed concrete (SFRSC). The possibility of obtaining and comparing constitutive models from these tests is verified in line with current trends to obtain design parameters for FRSC structures.

2. Methodology

2.1 Materials and spraying process

The concrete mixture was formulated with 400 kg/m^3 of cement (70% CEM I 52.5 R and 30% blast furnace slag), 574 kg/m^3 of fine quartz sand (0 - 0.6 mm), 315 kg/m^3 of crushed granitic sand (0 - 4.8 mm), 840 kg/m^3 of crushed granite coarse aggregate (4.8 - 12.5 mm) and 200 l/m^3 of water. The following admixtures were also added to the composition to ensure adequate fresh state properties: 1.44 kg/m^3 of polyfunctional admixture, 0.84 kg/m^3 of superplasticiser and 1.12 kg/m^3 of hydration stabiliser. The materials were batched in a ready-mix plant and supplied in a concrete mixer truck.

A flat crimped steel fibre was used in the experimental program. This is a low-cost fibre, produced from recycled steel wires and is commonly used in tunnel lining applications in Brazil. The dimensional characterization of length (L), equivalent diameter (d_e) and aspect ratio (λ) of the fibre

is presented in Table 1. The mean values, coefficient of variation (*CV*), standard deviation (*SD*) and sample size (*N*), are also provided.

The fibres were added directly to the mixer truck in three stages aiming to achieve three levels of fibre contents and mixed for at least 5 minutes in each stage. From the concrete mixer truck, the FRC was transferred to a wet-mix CP 10-SU pump and sprayed on wooden moulds positioned at 20° with the vertical axis. An accelerator admixture based on aluminium sulphate solution (approximately 24 kg/m^3) was used to ensure appropriate setting times, seeking to replicate the wet-mix sprayed process normally found in tunnel linings.

The sprayed panels were of two sizes. Small panels of 600 mm x 600 mm at the base, 800 mm x 800 mm at the top, and thickness of 100 mm; and large panels of 600 mm x 600 mm at the base, 1000 mm x 1000 mm at the top, and thickness 200 mm. Five small panels and one large panel were sprayed with a lower nominal fibre content (30 kg/m^3), and 6 small panels and one large panel with the intermediate and higher nominal fibre contents of 60 and 80 kg/m^3, respectively.

After the production of the first series of panels with the lower nominal fibre content, the volume of concrete remaining was estimated, and an extra amount of fibre was added to the mixer truck to reach the intermediate nominal fibre content. Once the panels were sprayed, the remaining volume was estimated again, and fibres were added to the mixer truck to achieve the highest nominal fibre content. Material remaining from previous spraying on both the pump and the hose complicated the control of the fibre addition process in the sprayed specimens. However, ensuring previously the exact fibre content is not essential for conducting the study as long as the same conditions are applied to the batch of specimens subjected to the different tests. The actual average fibre content incorporated was determined through samples extracted from the panels and using the inductive test (Torrents *et al*. 2012; Cavalaro *et al*. 2015; Cavalaro *et al*. 2016) and crushing of specimens (Kalil; Escariz; Figueiredo, 2010), as described in section 2.3. After the spraying, the test panels were covered with plastic sheets, were periodically sprayed with water and demolded three days later.

Table 1 *– Fibre dimensional characterization.*

	L (mm)	***d_e (mm)***	***$\lambda = L/d_e$***
Mean	38.93*	1.56	25.03
SD	1.16	0.06	1.12
CV (%)	0.03	0.04	0.04
N	60	60	60

* This value is within the dimensional tolerances of Brazilian standard ABNT NBR 15530 as the deviation from nominal length (L_n = 39 mm) is less than ±5% and ±1.5 mm. The other nominal values were not provided by the manufacturer.

2.2 Extraction of samples and preparation of specimens

18 cylinders with nominal dimensions Ø150 mm × 150 mm and 84 of Ø100 mm × 100 mm for the DPT were extracted from the large and small panels, respectively (see Figure 1a). To obtain the desired specimen height, the ends of the cylindrical cores were cut, removing the rough part. Twelve beams with nominal dimensions of 600 mm length, 125 mm wide and 75 mm high for the EN 14488-

3 test were cut from the small panels, from which no cylinders had been extracted (see Figure 1b). After testing the beams, their ends were cut at the extremes far enough from the cracked plane, into smaller prisms, 125 mm length, 75 mm wide and 125 mm high used in the DEWS test (see Figure 1c). To induce cracking in these small prisms, a notch and wedges were made in the middle of the top and bottom faces of the specimens (see Figure 1d). Then, steel plates were glued over the wedges to ensure smoother metallic contact with the load application rollers.

All specimens were prepared and tested at an age greater than 5 months to ensure enough time for extraction and preparation of all specimens. This also contributes to a minimum impact of the evolution of strength over time in the test results. The notations used to present the results are LB, SB, F and D, corresponding to the large cylinders Ø150 mm × 150 mm of the DPT, small cylinders Ø100 mm × 100 mm of the DPT, beams of the EN 14488-3 test and prisms of the DEWS test, respectively. The numbers following the notation refer to the nominal fibre content. For example, F_60 are the beams of the EN 14488-3 test with a nominal fibre content of 60 kg/m^3.

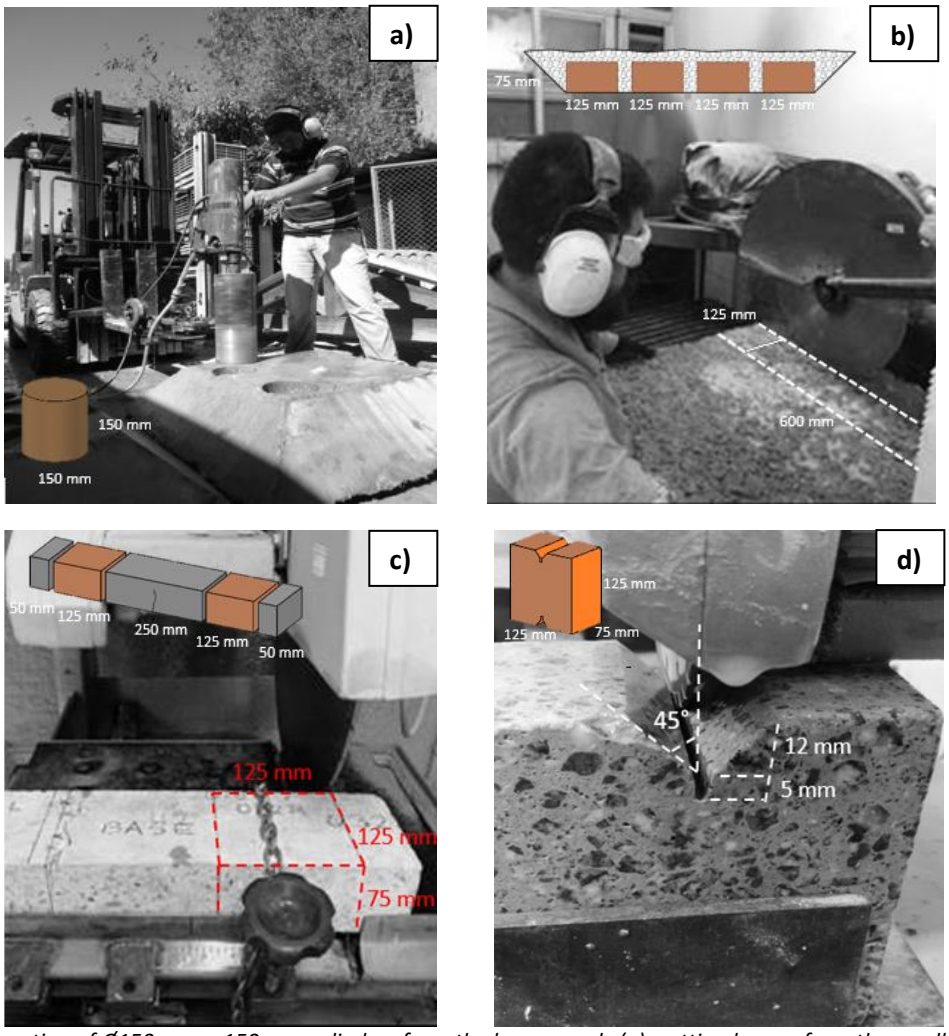

***Figure 1**: Extraction of Ø150 mm × 150 mm cylinders from the large panels (a); cutting beams from the small panels (b); cutting smaller prisms for the DEWS test (c); and making the wedge and notch in the DEWS prism (d).*

2.3 Determination of fibre content

The fibre content in the cylinders of the DPT was determined by the inductive test (Torrents *et al*. 2012; Cavalaro *et al*. 2015; Cavalaro *et al*. 2016). This methodology was previously used to quantify the fibre content in cores extracted from FRSC in the studies by Segura-Castillo *et al*. (2018) and Galobardes *et al*. (2019). Initially, a calibration process was performed on styrofoam cylinders, three of Ø100 mm × 100 mm (785.40 cm^3) and three of Ø150 mm × 150 mm (2650.72 cm^3), in which the fibre contents of 30, 60 and 90 kg/m^3 were inserted manually and randomly distributed in the volume of the cylinder. The inductance variation can be used to calculate the inductance coefficients of the fibre used, as described in Cavalaro *et al*. (2016). Figure 2 shows the correlations between the fibre content placed in the styrofoam cylinders and the sum of the inductance variation ΔL_T, measured in three orthogonal axes L_i.

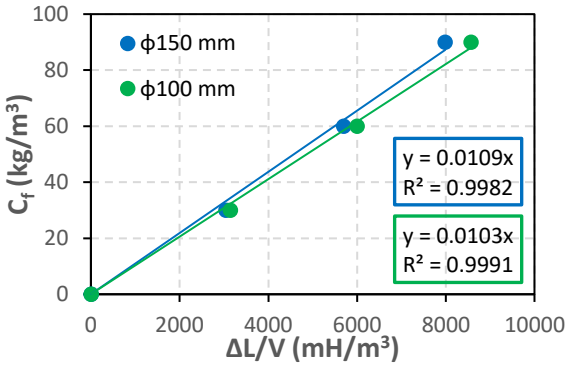

***Figure 2**: Inductive method calibration in styrofoam cylinders of Ø150 mm × 150 mm and Ø100 mm × 100 mm.*

Equation 1 provides the fibre content in the cylinders (C_f) in kg/m³, which depends on the coefficient β' (0.0109 and 0.0103 for the large and small cylinders, respectively), the total inductance variation (ΔL_T) in mH and volume of the cylinder (V) in m^3. The inductive test was performed on the cylinders prior to the DPT tests.

$$C_f = \beta' \times \frac{\Delta L_T}{V} \quad (1)$$

The average orientation number n_i on each orthogonal axis was calculated using Equation 2, where: $B_{V,i}$ is a constant that depends on the magnetic field over the volume of the cylinder, $B_{V,x}$ = $B_{V,y}$ are equal to 536 and 1789 for small and large cylinders, respectively; $B_{V,z}$ is equal to 538 and 1809 for small and large cylinders, respectively; γ is an inductance parameter that depends on the fibre aspect-ratio, which was assumed as 0.05 following the recommendation from Cavalaro *et al*. (2016); L_i is the inductance measurement on a specific axis; L_e is the sum of the ratio between each L_i measured in each of the orthogonal axis and the corresponding constant $B_{V,i}$. The fibre contribution C_i in each axis was determined according to Cavalaro *et al*. (2016) and was calculated using Equation 3. This parameter measures the average cosine of the angle formed by the fibres with the axis analysed. Fibres present the highest contribution to the inductance variation when parallel to the magnetic field (Cavalaro *et al*., 2016).

198 $$n_i = 1.03.\sqrt{\frac{L_i.(1+2\gamma)-L_e.B_{V,i}.\gamma}{L_e.B_{V,i}.(1-\gamma)}} - 0.85 \quad (2)$$

199 $$C_i = \frac{n_i}{\sum_{i=x,y,z} n_i} \quad (3)$$

200

201 The fibre content in the prisms used in the DEWS test was determined by crushing the specimens
202 and collecting fibres with a magnet after being tested, according to the procedure proposed by Kalil;
203 Escaris; Figueiredo (2010). The actual fibre content of the beams was determined considering the
204 average value obtained with the crushing of the two prisms cut from the end of the beams. The
205 crushing method was adopted since the prisms have a different geometry than a cylinder or cube,
206 which are considered in the inductive method by Cavalaro *et al*. (2016). Both methods have a good
207 approximation of results in the determination of fibre content (R^2 = 0.98) (Cavalaro *et al*., 2015).

208

209 **2.4 Flexural beam test EN 14488-3**

210 Ten beams were tested according to EN 14488-3 (three beams for each fibre content, plus one extra
211 for the nominal content of 60 kg/m^3). Two beams were lost due to rupture outside the central third,
212 one in the nominal content of 30 and 80 kg/m^3, respectively. The test was performed in a universal
213 INTERMETRIC IM750SRV testing machine using a closed-loop system. All beams were positioned in
214 the testing machine with the faces that were in contact with the mould in contact with the lower
215 rollers. The load was applied using two upper rollers, positioned over the central third of the beam
216 (see Figure 3). The displacement rate was 0.25 ± 0.05 mm/min until 0.5 mm when the rate was
217 increased to 1.0 mm/min until the end of the test. The vertical displacement measurements were
218 made using two LVDTs located in the central part at the top on each side of the beam and fixed to
219 a yoke.

220 The flexural strengths were obtained according to Equation 4, where: f_{Rim} is the residual strength;
221 P_δ is the load related to several displacements; *L* is the test span (450 mm); *b* is the beam width; *d*
222 is the height of the beam. The vertical displacement was transformed into a crack-opening
223 displacement (COD) at the base of the beam, using Equation 5, which was proposed by Carmona
224 and Molins (2019). Where: δ is the vertical displacement; *h* is the height of the beam; *L* is 450 mm;
225 and *e* is the crack eccentricity of the tested beam concerning the middle of the span.

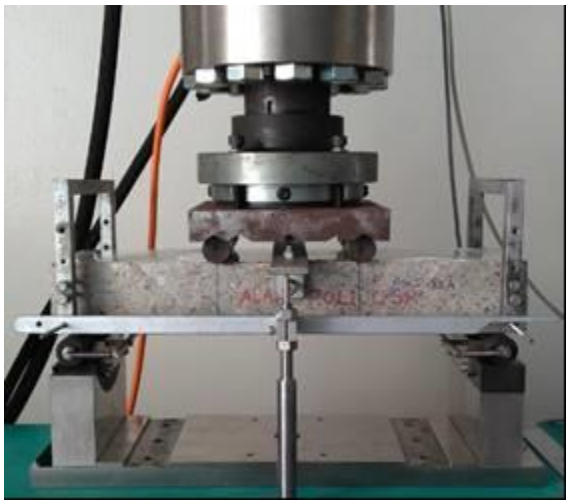

***Figure 3**: Flexural beam test according to EN 14488-3.*

$$f_{Rim} = \frac{P_{\delta}.L}{b.d^2} \quad (4)$$

$$COD = \frac{4.\delta.h}{(L-2.e)} \quad (5)$$

2.5 DPT

The DPT was performed on 18 large cylinders (Ø150 mm × 150 mm) and 83 small ones (Ø100 mm × 100 mm). Six large cylinders from each nominal content (six per panel). 23 small cylinders from the nominal content of 30 kg/m^3 (six per panel, minus 1 that was discarded), 30 from the nominal contents of 60 and 80 kg/m^3, respectively (six per panel). The test was carried out on a 200 tf universal Shimadzu machine in an open-loop system, according to the recommendations of Pujadas *et al*. (2013).

The punching load was applied using steel discs, with a diameter of 25 mm and a height of 20 mm for the small cylinders, and a diameter of 37.5 mm and a height of 30 mm for the large cylinders (maintaining the proportion specimen-steel disc diameter 1:4), arranged on their upper and lower plane faces (see Figure 4). The load was applied uniformly with a constant displacement rate of 0.5 ± 0.05 mm/min. The cylinders were always kept in the same position, the faces that were in contact with the mould were placed on the base of the machine. The residual strength of the FRSC is calculated according to Equation 6, proposed by Saludes (2006), where: $f_{R,\delta p}$ is the residual strength for a vertical displacement δ_p; $P_{\delta p}$ is the residual load for a vertical displacement δ_p; a is the diameter of the steel disc; H is the height of the cylinder.

In the original test setup, the increment of the perimeter TCOD (total circumferential opening displacement) was measured by a circumferential extensometer positioned at half the height of the cylinder. To simplify the procedure and facilitate implementation in quality control, Pujadas *et al*. (2013) proposed a model that converts the vertical displacement of the testing machine into the TCOD without the need for the circumferential extensometer.

Residual strength was calculated in different circumferential deformations TCOD. To transform the vertical displacement of the machine (δ_p) into TCOD, Equations 7 and 8 proposed by Pujadas *et al*. (2013) were used. Where: *n* is the number of radial cracks formed in the test; *a* is the diameter of the steel disc; *l* is the length of the wedge formed under the steel discs, 26.8 mm and 40.2 mm for the small and large cylinders, respectively; *P* is the load at the calculated point; P_{cr} and $\delta_{p,cr}$ are the load and vertical displacement at the maximum load point, respectively; $P_{R,0}$ and $\delta_{p,R,0}$ are the load and the vertical displacement at the starting point of the residual strength, respectively.

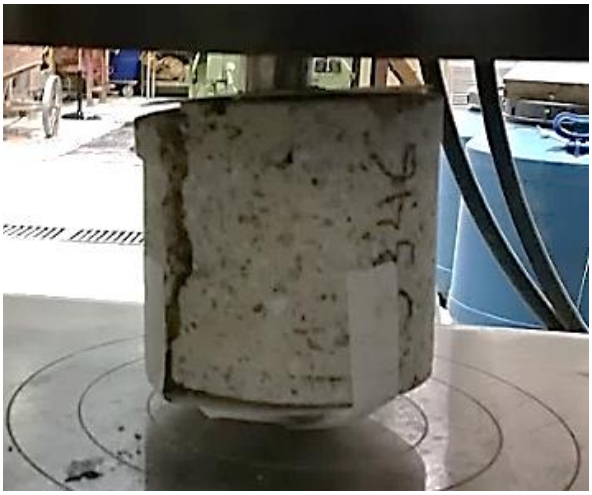

***Figure 4**: DPT on a small cylinder with a height and diameter of 100 mm.*

$$f_{R,\delta p} = \frac{4.P_{\delta p}}{9.\pi.a.H} \quad (6)$$

$$TCOD = n.\frac{a.\delta_{p,R,0}}{2.l}.\sin\frac{\pi}{n}.\left(1 - \frac{P}{P_{cr}}\right), \quad \delta_{p,cr} < \delta_p < \delta_{p,R,0} \quad (7)$$

$$TCOD = n.\frac{a}{2.l}.\sin\frac{\pi}{n}.\left[\delta_p - \delta_{p,cr} + \delta_{p,R,0}.\left(1 - \frac{P_{R,0}}{P_{cr}}\right)\right], \ \delta_p > \delta_{p,R,0} \quad (8)$$

2.6 DEWS test

The DEWS test was performed on six specimens per each nominal content. The nominal content of 60 kg/m^3 was analyzed with five specimens as one was discarded. The test was performed on an EMIC DL 10000 universal machine with a capacity of 100 kN in an open-loop system, according to the recommendations of Borges *et al*. (2019). The loading speed was 0.12 mm/min until the matrix cracked, and 0.30 mm/min from the point of the first crack until the end of the test. The crack-opening displacement was measured by an LVDT positioned on each face of the specimen. The crack-opening *w* was the average of the measurements of the two LVDTs (see Figure 5).

The parameters provided by the machine were load versus crack-opening. The tensile strength was obtained according to Di Prisco; Ferrara; Lamperti (2013). The effective load acting on the specimen

P_{ef} was calculated using Equation 9, where: P is the load applied by the test machine; μ is the friction coefficient between the cylindrical rollers and the steel plates, the value adopted was 0.15; Θ is the angle formed between the wedge surface and the notch centre line, that is 45°. The tensile strength σ was calculated using Equation 10, where: P_{ef} is the effective load; b is the width of the cross-section of the specimen; h_{lig} is the distance between the ends of the two notches.

***Figure 5**: DEWS test performed on a prismatic specimen extracted from the beams.*

$$P_{ef} = P.\frac{(\cos\theta - \mu.\sin\theta)}{(\sin\theta + \mu.\cos\theta)} \quad (9)$$

$$\sigma = \frac{P_{ef}}{b.h_{lig}} \quad (10)$$

3. Results and analysis

3.1 Effective fibre content

Table 2 shows the results of average fibre content (C_f) obtained by the inductive test and crushing the specimens. Table 3 shows the average fibre incorporation in each axis (C_i) by the inductive test. The standard deviation (*SD*), coefficient of variation (*CV*), and sample size (*N*) are also provided in both tables.

***Table 2** - Fibre content (C_f) in kg/m³ by the inductive test and crushing.*

	C_f in kg/m³ by the inductive test						***C_f in kg/m³ by crushing***					
	DPT Ø100 × 100 mm			***DPT Ø150 × 150 mm***			***EN 14488-3 beams***			***DEWS prisms***		
	SB_30	***SB_60***	***SB_80***	***LB_30***	***LB_60***	***LB_80***	***F_30***	***F_60***	***F_80***	***D_30***	***D_60***	***D_80***
Mean	34	63	75	47	80	77	29	55	77	28	54	78
SD	4	7	10	2	6	9	3	3	5	3	4	4
CV (%)	13	12	14	5	7	11	12	6	7	10	8	5
N	23	30	30	6	6	6	3	4	3	6	5	6

Table 3 *- Fibre incorporation on each axis (C_x, C_y, C_z) by the inductive method.*

DPT Ø150 mm × 150 mm									
	LB_30			***LB_60***			***LB_80***		
	C_x	C_y	C_z	C_x	C_y	C_z	C_x	C_y	C_z
Mean	0.35	0.38	0.27	0.38	0.36	0.26	0.39	0.41	0.20
SD	0.02	0.02	0.03	0.03	0.02	0.02	0.02	0.04	0.02
CV (%)	0.07	0.04	0.11	0.07	0.04	0.08	0.06	0.09	0.08
N	6	6	6	6	6	6	6	6	6
DPT Ø100 mm × 100 mm									
	SB_30			***SB_60***			***SB_80***		
	C_x	C_y	C_z	C_x	C_y	C_z	C_x	C_y	C_z
Mean	0.39	0.37	0.24	0.38	0.37	0.25	0.40	0.40	0.20
SD	0.04	0.04	0.02	0.03	0.03	0.03	0.03	0.03	0.03
CV (%)	0.09	0.10	0.10	0.07	0.09	0.14	0.09	0.07	0.15
N	23	23	23	30	30	30	30	30	30

Table 2 shows that there was a natural variation in the fibre content incorporated in the elements compared to the nominal content due to the spraying process and phenomenon of rebound. Despite that, for each nominal content, the fibre incorporated in the specimens remains nearly in the same range. However, the DPT on large cylinders LB_30 and LB_60 show higher contents, due to the increase caused by the uncertainty around the remaining material in the machine pump and hose.

It is noted that the DPT in small cylinders has a higher *CV* compared to other specimens. This greater variation is associated with the small volume of the specimen and by the fact that the fibre used has a low aspect-ratio (λ = 25), which implies a smaller number of fibres present in the sample. The *CV* might also have increased because these cylinders were extracted from different panels.

Table 3 shows that the smallest fibre contribution is found in the plane parallel to the spraying direction (C_z), mean value of 0.24. The fibre contribution in the *x* and *y* axes (C_x and C_y) are similar, both with a mean value of 0.38. The sum of C_x and C_y assesses the XY in-plane fibre contribution parallel to the surface equal to 0.76, that is consistent with those by Segura-Castillo *et al*. (2018) and Galobardes *et al*. (2019) who found 0.85 and 0.80, respectively. The high degree of anisotropy is caused by the effect of the spraying process, which tends to align fibres parallel to the spraying surface (Banthia; Trottier; Beaupré, 1994; Robins; Austin; Jones, 2003).

3.2 Strength results

The load-displacement curves of the EN 14488-3 test, DPT in large and small cylinder, and the load-crack opening curves of the DEWS test are shown in Figure 6. All curves were considered from the peak load using the same criteria adopted by Nogueira *et al*. (2020). These curves were converted into stress-crack opening curves utilizing Equations 4 to 10. The average stress-crack opening curves are shown in Figure 7. The mean values, the standard deviation (*SD*), the coefficient of variation (*CV*) and the sample size (*N*) of the maximum and residual strength results are provided in Table 4.

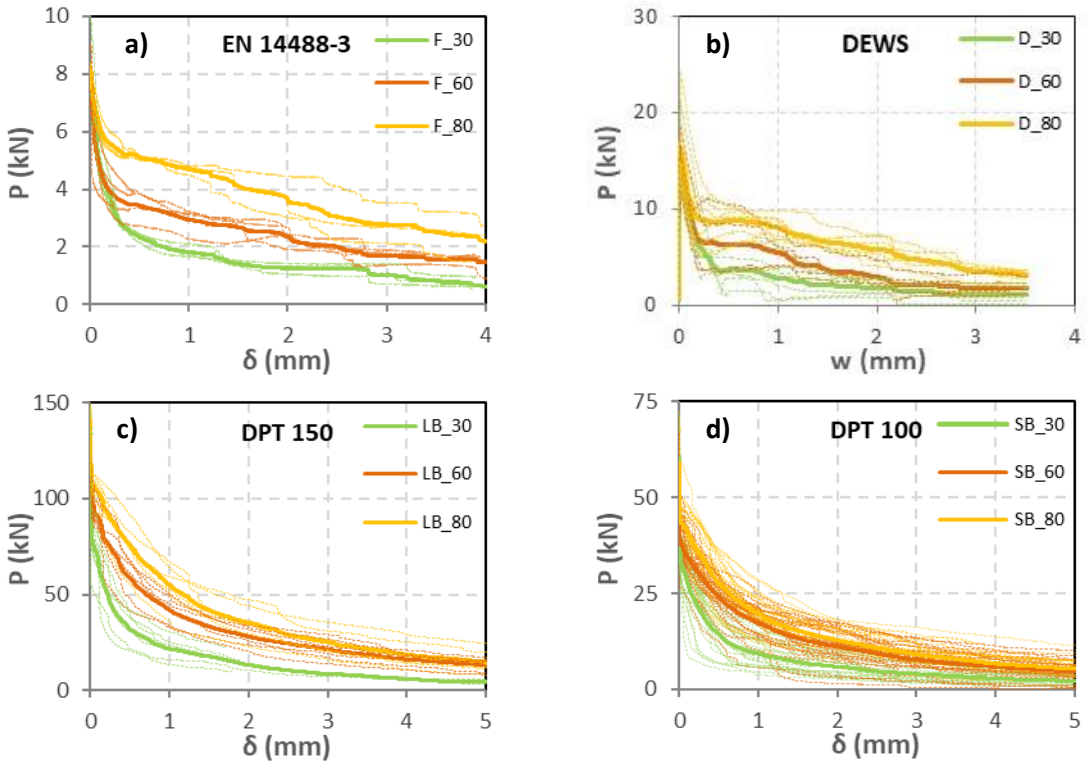

Figure 6 – *Load-displacement curves by the flexural beam test EN 14488-3 (a); load-crack opening curves by the DEWS test (b); and load-displacement curves by the DPT in a large – DPT 150 (c) and small – DPT 100 (d) cylinder. The average curves are shown in continuous lines.*

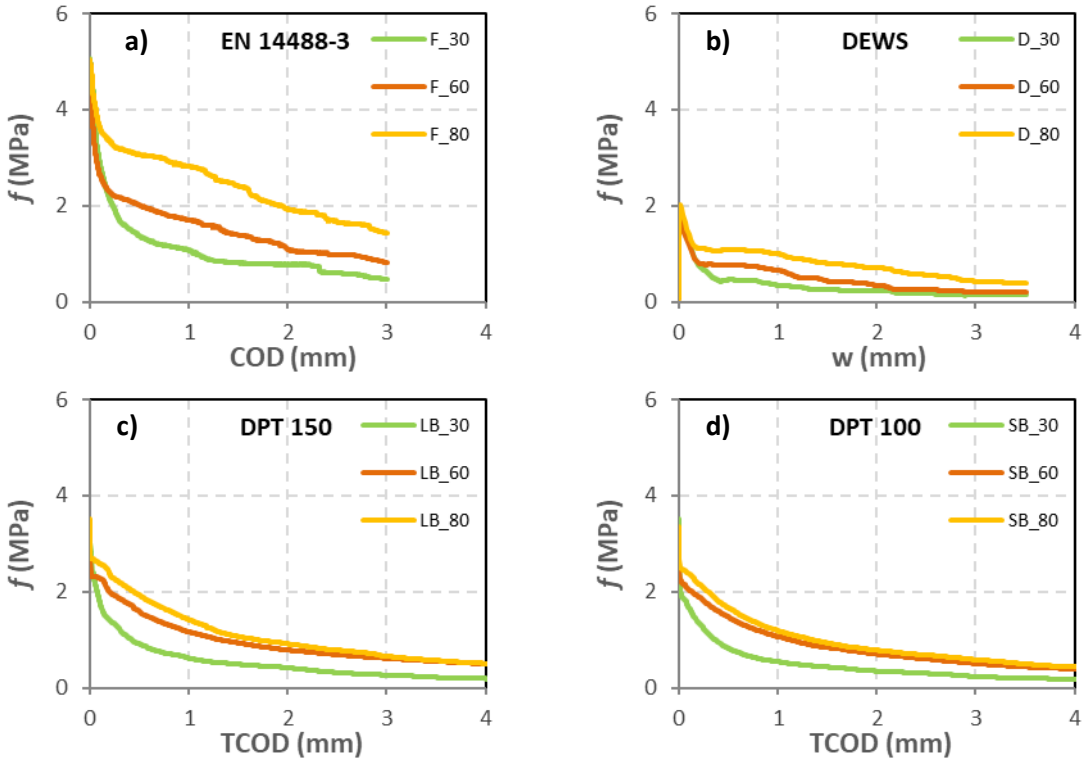

Figure 7 - *Average strength-COD curves by the flexural beam test EN 14488-3 (a); average strength-w curves by the DEWS test (b); average strength-TCOD curves by the DPT in the large – DPT 150 (c) and small – DPT 100 (d) cylinder.*

***Table 4**: Maximum strength (f_{max}) and residual strengths results at crack-openings of 0.5, 1.5 and 2.5 mm ($f_{0.5}$, $f_{1.5}$, $f_{2.5}$) in MPa, for flexural beam test EN 14488-3, DEWS test, DPT in a large (Ø 150 mm × 150 mm) and small (Ø 100 mm × 100 mm) cylinder.*

Flexural beam test EN 14488-3 - f (MPa)												
	F_30				***F_60***				***F_80***			
	f_{max}	$f_{0.5}$	$f_{1.5}$	$f_{2.5}$	f_{max}	$f_{0.5}$	$f_{1.5}$	$f_{2.5}$	f_{max}	$f_{0.5}$	$f_{1.5}$	$f_{2.5}$
Mean	5.1	1.4	0.8	0.6	5.0	2.0	1.4	1.0	5.0	3.1	2.4	1.7
SD	1.0	0.2	0.1	0.2	0.5	0.3	0.2	0.1	0.2	0.2	0.2	0.2
CV (%)	19	15	15	29	10	13	13	6	3	7	7	13
N	3	3	3	3	4	4	4	4	3	3	3	3
DEWS test - f (MPa)												
	D_30				***D_60***				***D_80***			
	f_{max}	$f_{0.5}$	$f_{1.5}$	$f_{2.5}$	f_{max}	$f_{0.5}$	$f_{1.5}$	$f_{2.5}$	f_{max}	$f_{0.5}$	$f_{1.5}$	$f_{2.5}$
Mean	1.8	0.5	0.3	0.2	1.7	0.8	0.4	0.3	2.0	1.1	0.8	0.6
SD	0.4	0.2	0.2	0.1	0.3	0.4	0.2	0.1	0.5	0.2	0.1	0.1
CV (%)	21	49	60	66	19	50	35	47	24	22	12	17
N	6	6	6	6	5	5	5	5	6	6	6	6
DPT Ø150 mm × 150 mm - f (MPa)												
	LB_30				***LB_60***				***LB_80***			
	f_{max}	$f_{0.5}$	$f_{1.5}$	$f_{2.5}$	f_{max}	$f_{0.5}$	$f_{1.5}$	$f_{2.5}$	f_{max}	$f_{0.5}$	$f_{1.5}$	$f_{2.5}$
Mean	3.4	0.9	0.5	0.3	2.9	1.6	0.9	0.7	3.5	1.9	1.1	0.8
SD	0.2	0.3	0.1	0.1	0.3	0.3	0.2	0.2	0.1	0.3	0.3	0.3
CV (%)	6	28	28	20	9	21	19	22	3	16	26	35
N	6	6	6	6	6	6	6	6	6	6	6	6
DPT Ø100 mm × 100 mm - f (MPa)												
	SB_30				***SB_60***				***SB_80***			
	f_{max}	$f_{0.5}$	$f_{1.5}$	$f_{2.5}$	f_{max}	$f_{0.5}$	$f_{1.5}$	$f_{2.5}$	f_{max}	$f_{0.5}$	$f_{1.5}$	$f_{2.5}$
Mean	3.5	0.9	0.5	0.3	3.1	1.5	0.8	0.6	3.4	1.7	0.9	0.7
SD	0.3	0.4	0.2	0.2	0.4	0.3	0.3	0.3	0.4	0.4	0.3	0.2
CV (%)	8	40	44	47	14	21	36	43	12	24	29	31
N	23	23	23	23	30	30	30	30	30	30	30	30

From Figures 6-7, all curves present strain-softening behaviour. In general, it appears that the residual strength increases with the fibre content, thus obeying a fundamental technological aspect of the FRC: the higher the fibre content, the greater the number of fibres acting as a stress transfer bridge at the crack (Bentur; Mindess 2007). From Table 4, considering the peak-load strengths, the highest *CV* is presented in DEWS test (mean *CV* = 21%). The flexural beam test EN 14488-3 and DPT in small cylinder show nearly the same variation (mean *CV* = 11%). The DPT in large cylinder has the lowest variation (mean *CV* = 6%). This can be attributed to the larger fracture surface and to the greater robustness of the cylinder in relation to the other specimens, having a greater capacity to absorb the rupture energy.

Greater cracking load tends to be achieved in larger specimens due to their bigger fracture surface. This should lead to bigger pre-cracking energy absorption in large cylinder as opposed to the observed in other specimens. As the cracking area increases, the number of fibres also increases, leading to bigger resistant load and energy absorption capacity. As observed by Cavalaro and Aguado (2015), the variability in the total number of fibres mobilised reduces with the increase of

348 the cracked section. Therefore, larger cracking area should lead to smaller coefficient of variation in
349 terms of resistant load and energy absorption.

350 Considering the residual strengths in the crack-openings evaluated, the largest *CVs* are shown in the
351 DEWS test (mean *CV* = 40%) and DPT in small cylinder (mean *CV* = 35%). This can be justified by the
352 smaller fracture surface, exacerbated by the scarce number of fibres crossing the cracking sections,
353 since the fibre has a low aspect-ratio (λ = 25). In an intermediate situation is found the DPT in large
354 cylinder that has the larger fracture surface (mean *CV* = 24%). Even with small fracture surface, the
355 lowest *CV* is shown in the flexural beam test EN 14488-3 (mean *CV* = 13%). This can be justified
356 because this test was the only one performed on a machine with a closed-loop system, thus reducing
357 the effect of post-cracking instability. In almost all tests, the *CV* decreases as the fibre content
358 increases, except for the DPT in large cylinder, which presents an almost constant *CV* in the
359 evaluated mixtures, around 24%. The variation in the number of fibres could be one of the causes
360 of the behaviour observed, albeit a conclusive answer could not be achieved based on the data
361 available.

362

363 **3.3 Comparative analysis of strength results**

364 As expected, there is no influence of the fibre content in the maximum strengths as the softening
365 behaviour was observed (Bentur; Mindess, 2007). Figure 8a shows the comparison of individual
366 results of maximum strengths obtained from different tests associated with the actual fibre content.
367 The average strengths are shown in continuous lines. Confidence intervals, obtained according to
368 the method of Freund and Simon (2002) for a 90% confidence, are shown in dashed lines. The
369 highest mean strength (5.03 MPa) was obtained in flexural beam test EN 14488-3, followed by DPT
370 in large and small cylinder (both with mean strength of 3.29 MPa), the lowest mean strength was
371 obtained in DEWS test (1.86 MPa). It is noticed that the mean strength of the DEWS test is almost a
372 third of that obtained in the flexural beam test. According to the *fib* Model Code (2010) in a rigid
373 plastic linear model, the uniaxial tensile strength could be considered as a third of the flexural
374 strength.

375 Figure 8b, 8c and 8d show the comparison of individual results of residual strengths by fibre content
376 at crack-openings of 0.5, 1.5 and 2.5 mm. The linear regressions are shown on continuous lines and
377 the confidence intervals on dashed lines. All correlations are linear and pass through the origin. The
378 highest correlation is obtained in the flexural beam test EN 14488-3 (R^2 between 0.98 and 0.99),
379 followed by the DPT in large cylinder (R^2 between 0.93 and 0.96). The DPT in small cylinder and the
380 DEWS test have the lowest correlation, R^2 between 0.89 and 0.95 the former and between 0.90 and
381 0.94 the latter. The highest strengths were obtained in the flexural beam test EN 14488-3, followed
382 by the DPT in large and small cylinders, which practically maintain the same trend line. This shows
383 that any of the specimen sizes subjected to the DPT here can be used in the evaluation of residual
384 strength, as they provide similar results. The lowest strengths correspond to the DEWS test.

To test the equality of the residual strengths of the DPT in the large and small cylinder, a t-student statistical analysis was performed, comparing the means of the two samples (H_0: $\mu_1 = \mu_2$), with a confidence of 95% ($t_{tabulated}$ 1.96). The $t_{calculated}$ values of the residual strengths for the crack-openings at 0.5, 1.5 and 2.5 mm were: 0.76, 0.75 and 0.67, respectively, being within the acceptance region ($t_{calculated} < t_{tabulated}$), thus proving the equality of the population averages.

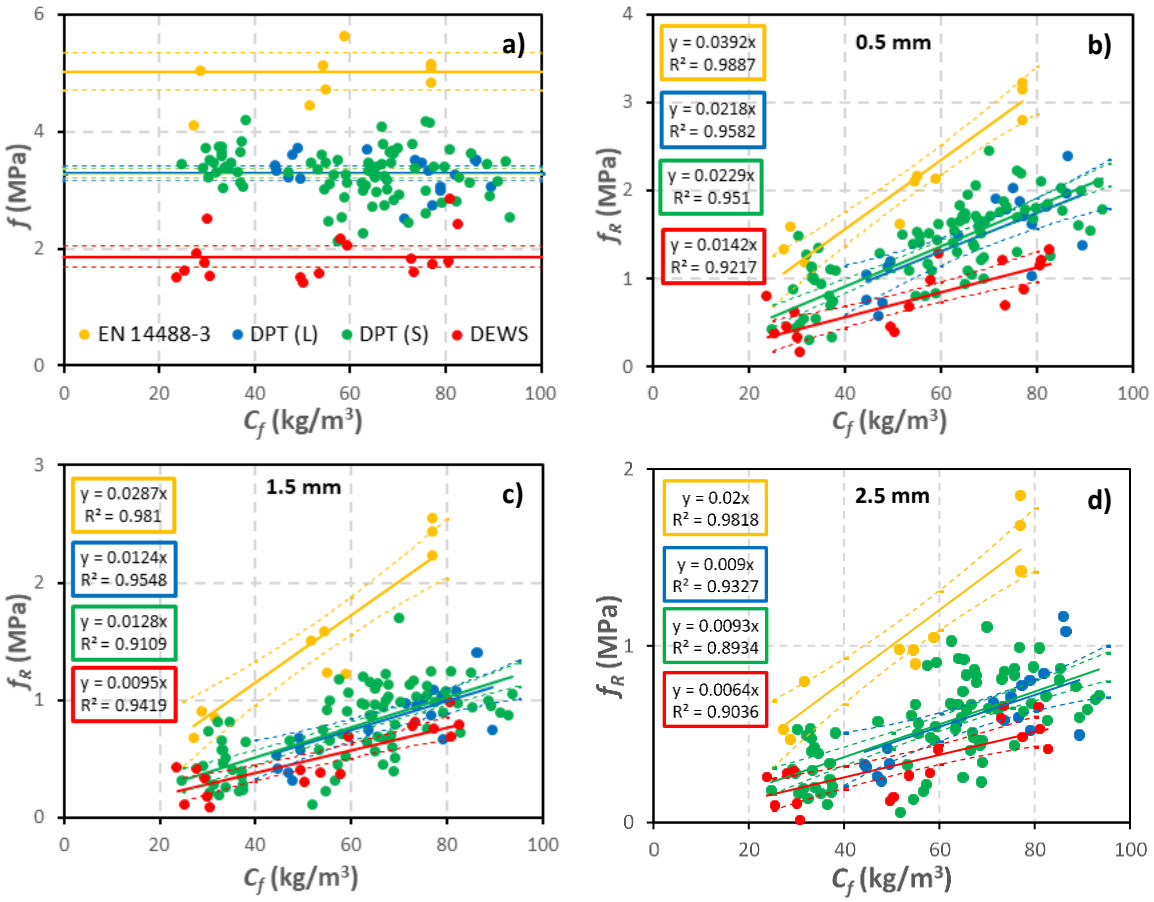

Figure 8 *- Comparison of maximum strengths (a); and residual strength results at 0.5 mm (b), 1.5 mm (c) and 2.5 mm (d) crack-openings by fibre content between the flexural beam test EN 14488-3, DPT in large - DPT (L) and small - DPT (S) cylinder and DEWS test.*

To correlate the tests, residual strengths were obtained from linear regression equation in Figure 8. Since the DPT on both cylinder sizes does not show significant differences, a single linear regression was adopted for each crack-opening considering both datasets. The linear regression equations were: at 0.5 mm (y = 0.0227x), at 1.5 mm (y = 0.0127x) and at 2.5 mm (y = 0.0092x). Table 5 shows the residual strengths found for each crack-opening. Figure 9 shows the correlations obtained between the residual strengths obtained with the flexural test and the alternative tests.

***Table 5**: Residual strengths for each crack-opening ($f_{0.5\,mm}$, $f_{1.5\,mm}$, $f_{2.5\,mm}$) in MPa in fibre contents of 30, 60 and 80 kg/m³, according to the linear regression equations for EN 14488-3, DPT and DEWS tests.*

Residual strengths (MPa) according to the linear regression equations									
	$f_{0.5\,mm}$			$f_{1.5\,mm}$			$f_{2.5\,mm}$		
C_f (kg/m³)	**30**	**60**	**80**	**30**	**60**	**80**	**30**	**60**	**80**
EN 14488-3	1.2	2.4	3.1	0.9	1.7	2.3	0.6	1.2	1.6
DPT	0.7	1.4	1.8	0.4	0.8	1.0	0.3	0.6	0.7
DEWS	0.4	0.9	1.1	0.3	0.6	0.8	0.2	0.4	0.5

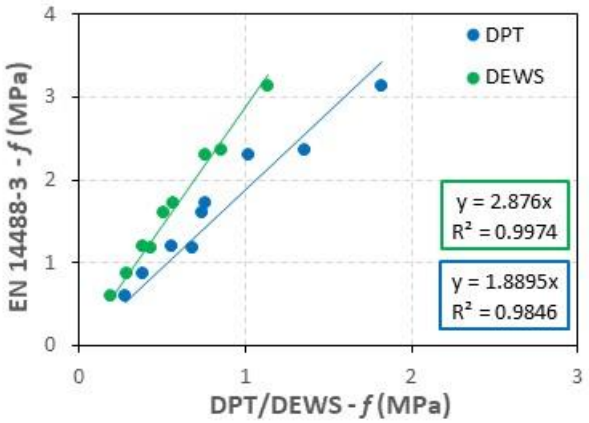

***Figure 9** - Correlation of the residual strength results between the EN 14488-3 test with DPT and DEWS tests.*

High correlations (R^2 above 0.98) were obtained between residual strength results of flexural beam test EN 14488-3 and alternative tests. The highest correlation was obtained with the DEWS test (R^2 = 0.997), a fact that can be justified because the specimens of this test were extracted from the ends of the beams used in the flexural test. Furthermore, in these two tests, there is no influence of the internal friction of the matrix, which produces results with less influence of intervening variables. The DPT has a slightly lower correlation, R^2 of 0.985. The excellent correlations obtained between the proposed new tests and the flexural beam test EN 14488-3 indicate that these tests could be used in the evaluation of the residual strength of the FRSC, replacing the EN 14488-3 test. Nevertheless, the DEWS test is the most promising due to the advantage of being a test with a type I fracture, directly providing the results of tensile strength by crack-opening. The following section shows a more detailed assessment considering the post-cracking tensile results of the flexural beam test EN 14488-3, according to the parameters established in the *fib* Model Code (2010).

3.4 Comparison of constitutive models

Codes (RILEM, 2003, CNR, 2006; CPH 2008; *fib* Model Code, 2010) and studies (Lok; Xiao, 1998; Dupont, 2003; Vandewalle *et al*. 2003; Tlemat; Pilakoutas; Neocleous, 2006; di Prisco; Colombo; Dozio, 2013; Thai; Nguyen; Nguyen, 2020) establish constitutive models based on flexural beam tests for FRC. However, these references do not focus on FRSC. Since there is a current trend to transfer the approach of the *fib* Model Code to FRSC technology (ITA, 2020; Larive *et al*., 2020) to

obtain constitutive models for flexural beam test, it was considered necessary to apply the results of the EN 14488-3 test to *fib* Model Code parameters. The residual strengths of the EN 14488-3 test in Table 5 were converted into tensile strengths, using the constitutive equations of the *fib* Model Code (Equations 11 - 12). These equations describe a linear post-cracking with strain-softening behaviour (see Figure 10a), where: f_{FTs} and $f_{FT2.5}$ are the tensile strengths at 0 and 2.5 mm of crack-opening, respectively; f_{R1} and f_{R3} are the residual strengths of the flexural beam test in 0.5 and 2.5 mm, respectively. The results obtained from the tensile strength of the EN 14488-3 test are shown in Table 6. The post-cracking lines derived from these results are shown in Figures 11.

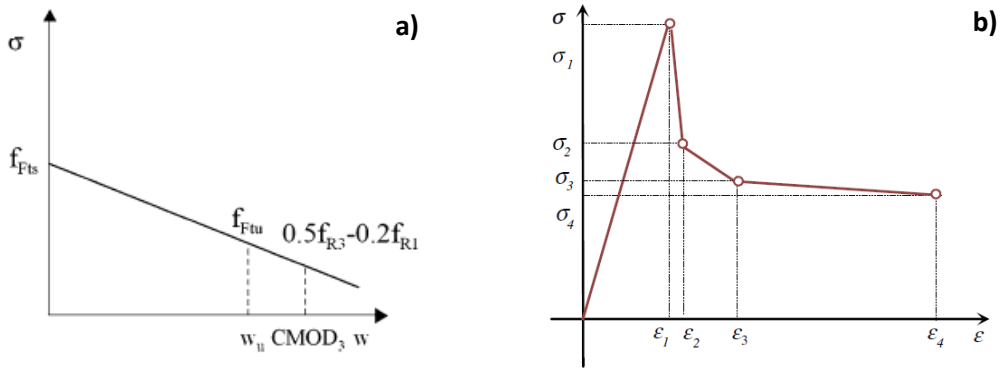

Figure 10 *– Linear post-cracking model by the fib Model Code (2010) utilized in the flexural beam test EN 14488-3 (a). Simplified diagram σ - ε of the constitutive model for the DPT by Blanco et al. (2014).*

$$f_{FTS} = 0.45 f_{R1} \quad (11)$$

$$f_{FT2.5} = 0.5 f_{R3} - 0.2 f_{R1} \quad (12)$$

Table 6*: Tensile strength results in MPa of flexural beam test EN 14488-3 according to fib Model Code (2010).*

EN 14488-3 - σ (MPa)			
C_f	***30 kg/m³***	***60 kg/m³***	***80 kg/m³***
F_{FTs}	0.5	1.1	1.4
$F_{FT2.5}$	0.1	0.1	0.2

To convert the strength results of DPT into tensile strength, it was necessary to use the constitutive equations proposed by Blanco *et al*. (2014). These equations describe the post-cracking behaviour of tensile strength by strain σ - ε at four levels of strain: ε_1, ε_2, ε_3, ε_4 (see Figure 10b). The increments of the strain $\Delta\varepsilon_i$ from the peak load are: $\Delta\varepsilon_1 = \varepsilon_2 - \varepsilon_1 = 0.1$ ‰, $\Delta\varepsilon_2 = \varepsilon_3 - \varepsilon_1 = 3.9$ ‰, $\Delta\varepsilon_3 = \varepsilon_4 - \varepsilon_1 =$ 19.9 ‰. The $\Delta\varepsilon_i$ were converted into vertical displacement increments $\Delta\delta_{Pi}$ using Equation 13, where: R is the radius of the cylinder; n is the number of radial cracks formed in the test; β is half the fracture angle of the conical wedge that appears under the load discs after performing the test, i.e. 25°. Thus, the vertical displacement increments for large cylinders (Ø150 mm x 150 mm) are: $\Delta\delta_{P1} = 0.02$ mm, $\Delta\delta_{P2} = 0.75$ mm and $\Delta\delta_{P3} = 4.00$ mm. According to the results obtained in the DPT on a larger cylinder, the $\Delta\delta_{Pi}$ correspond to $\Delta TCDO_{Pi}$ crack-opening increments of: $\Delta TCDO_{P1} = 0.03$ mm, $\Delta TCDO_{P2} = 0.92$ mm and $\Delta TCDO_{P3} = 4.87$ mm. In order to unify the results, since it was proved that there is no significant difference between the residual strengths of the DPT in large and small

cylinders and that they almost maintain the same trend line in Figure 8, these increments were adopted for both cylinder sizes.

The tensile strength corresponding to peak load σ_1 and each crack-opening increment from the peak load $\sigma_{\Delta TCODPi}$, were calculated according to Equations 14 and 15, which were adapted from Blanco *et al*. (2014). Where: F_{Pmax} is the peak load; $F_{\Delta TCODPi}$ is the load corresponding to the crack-opening increments Δ_{TCDOPi} from the peak load; β is 25°; μ_k is the kinetic friction coefficient, a value of 0.7 was adopted; and A is the radial value of the cracked surface. For the calculation of A, Equation 16 was used, where: d and H are the diameter and height of the cylinder, respectively; a is the diameter of the load application disc, that is, 37.5 mm for the large cylinder and 25 mm for the small cylinder; and β is 25 °.

Thus, the individual results of the tensile strength by fibre content of the DPT, which correspond to the peak load and the crack-opening increments Δ_{TCDOPi}, were calculated. With these results, linear regressions were performed passing through the origin, except for the peak load results, since this property depends on the concrete matrix. For this particular case, the average value was adopted. The tensile strength values at each Δ_{TCDOPi} were calculated through linear regression for the fibre contents of 30, 60 and 80 kg/m^3. The results are shown in Table 7. From these results, the post-cracking linear behaviour of the DPT was plotted (see Figure 11).

$$\Delta\delta_{Pi} = \frac{\Delta\varepsilon_i.\pi.R}{n.\tan\beta.\sin\frac{\pi}{3}} \quad (13)$$

$$\sigma_1 = \frac{F_{Pmax}}{2.\pi.A} \times \frac{\cos\beta - \mu_k.\sin\beta}{\sin\beta + \mu_k.\cos\beta} \quad (14)$$

$$\sigma_{\Delta TCOD_{Pi}} = \frac{F_{\Delta TCOD_{Pi}}}{2.\pi.A} \times \frac{\cos\beta - \mu_k.\sin\beta}{\sin\beta + \mu_k.\cos\beta} \quad (15)$$

$$A = \frac{d.H}{4} - \frac{a^2}{4.\tan\beta} \quad (16)$$

***Table 7**: Tensile strength results in MPa of the DPT according to the constitutive equations of Blanco et al. (2014).*

Δ_{TCODPi} (mm)	DPT - $\sigma_{\Delta TCODPi}$ (MPa)		
	30 kg/m³	60 kg/m³	80 kg/m³
0.00	1.9	1.9	1.9
0.03	0.6	1.2	1.6
0.92	0.3	0.6	0.8
4.87	0.1	0.2	0.2

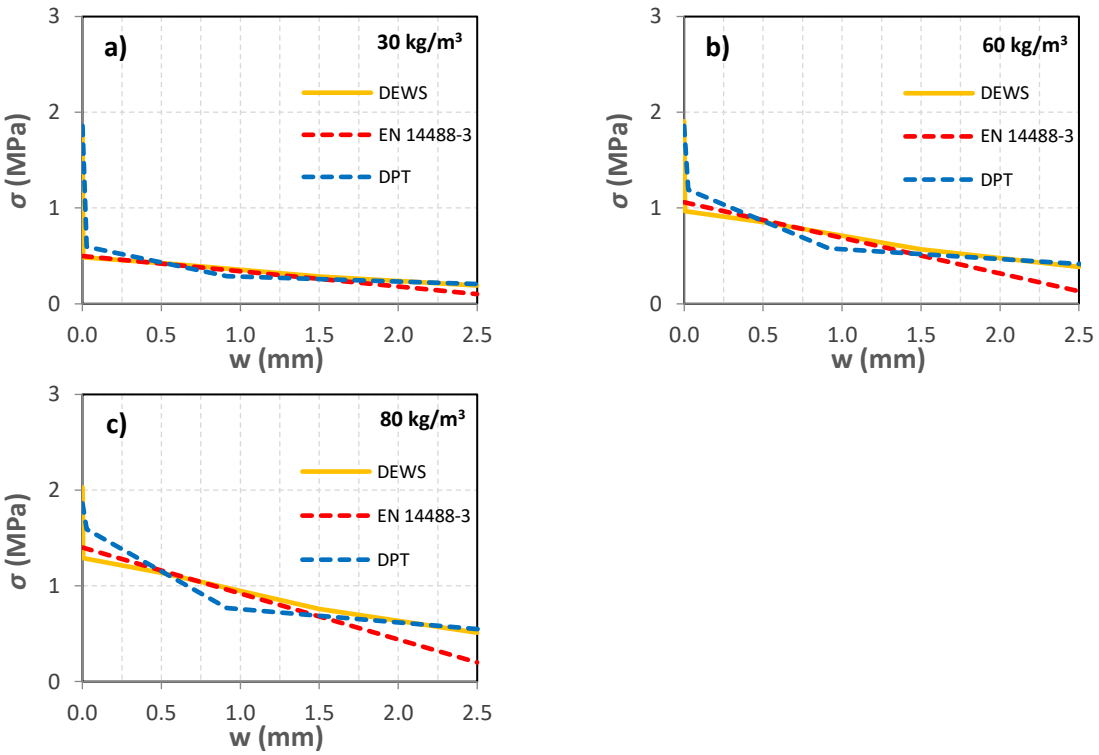

Figure 11 *- Comparison between the tensile strength results by crack-opening (σ - w) of flexural beam test EN 14488-3 according to the fib Model Code (2010), DPT according to the constitutive equations of Blanco et al. (2014) and DEWS test for fibre contents of 30 kg/m³ (a), 60 kg/m³ (b) and 80 kg/m³ (c).*

Besides the post-cracking linear behaviour of the DPT and EN 14488-3 test, Figure 11 also includes the lines that describe the post-cracking behaviour of the DEWS test in the contents of 30, 60 and 80 kg/m³, derived from strength results of Table 5. The stress-crack opening ($\sigma - w$) of all tests are similar. For crack openings bigger than 1.5 mm and the same fibre content, DEWS and DPT show similar results that are consistently bigger than those observed in the EN 14488-3 tests. The biggest difference between the tests is 0.3 MPa at 2.5 mm crack opening for the content of 80 kg/m³. For small crack openings (w < 1.5 mm) the EN 14488-3 and DEWS show similar results, which differ slightly from the values obtained with the DPT. Interestingly, all test methods show nearly the same results for 0.5 mm crack opening in each of the 3 fibre contents assessed here.

The good approximations of the linear post-cracking behaviour of the tests, confirm that the new proposals of tests in smaller-scale can substitute the flexural beam test EN 14488-3 according to the parameters of the *fib* Model Code. The DEWS has the advantage of being able to directly represent the tensile strength response by crack-opening, as if it were a uniaxial direct tensile test, due to the fracture type I that occurs in the specimens. The DPT on both cylinder sizes is also promising, but it is necessary to develop an analytical process using constitutive equations, to obtain the post-cracking response of tensile strength by crack-opening.

4. Conclusions

The highest *CV* in the residual strengths was observed in the DEWS test (mean *CV* = 40%) and DPT in small cylinder (mean *CV* = 35%). This can be attributed to the small fracture surface and by the type of fibre used with a low aspect-ratio (λ = 25). The DPT in large cylinder presented a mean *CV* of 24%, which remained almost constant for all mixtures. The flexural beam test EN 14488-3 showed the lowest mean *CV* of 13%. However, this test was the only one performed in a closed-loop system machine, thus reducing the effect of post-peak instability.

Although the high level of variation of results, high correlation factor were obtained with the flexural beam test EN 14488-3 and the alternative tests showing excellent parallelism. The DEWS test resulted in a R^2 correlation of 0.997 and is particularly compatible with the assessment of the constitutive curve used in the design. The DEWS presents fracture type I and the tensile strength results are obtained directly associate to crack-openings, similarly to an uniaxial direct tensile test. Therefore, the constitutive models could be obtained in a more simplistic way. However, the DEWS demands more time for the preparation of the specimens. Thus, this test becomes more suitable for studies prior to the execution of the work, in the assessment of the constitutive equations of the FRSC. Although the prisms of the DEWS test were obtained by cutting the ends of the tested beams, it is noteworthy that this test can also be carried out from cores extracted from panels or the structure.

The approach proposed in the study also showed that it is possible to predict the flexural beam test EN 14488-3 based on the results of the DPT on both cylinder sizes, since a high correlation was obtained (R^2 = 0.985). The DPT on cylinders with a height and diameter of 100 and 150 mm practically show the same trend in terms of residual strength by fibre content in the evaluated crack-openings. It was statistically proven that the residual strengths of both cylinders do not differ significantly. The constitutive models obtained for FRSC from the DPT results were also close to that of the EN 14488-3 test, although demanding a more complex analysis. This, in addition to the fact that the specimens require very little preparation, opens the possibility of using the DPT as a complementary and practical method in the control of FRSC structures, both in the routine control of tunnel execution or even for existing structures evaluation.

The tests commonly used to determine the residual strength of the FRSC by flexural beam test EN 14488-3 are complex, as the beams need to be cut from previously sprayed panels, which can weigh up to 110 kg, making handling difficult. This will be even more difficult if the EN 14651 is adopted because the specimens are larger.

The proposed correlations represent a simple FRSC control tool based on smaller-scale tests. The focus is also in line with the philosophy of the *fib* Model Code (2010) that prioritize the constitutive model use and can serve as an example for future correlations using other types of fibres. However, the correlations cannot be generalized. Further studies need to be done with different compressive strengths levels, other types of fibres and spraying at different angles.

Acknowledgements

The authors gratefully acknowledge for the collaboration of PδD ANEEL (Pesquisa e Desenvolvimento - Agencia Nacional de Energia Eletrica, Brasil) and Brazilian enterprises: CPB (Concreto Projetado Brasil), Solotrat Engenharia and Holcim Brasil. The authors are also grateful for the kind collaboration of Professor Marco Cárnio, who provided the machine to carry out the flexural beam test EN 14488-3. Alan Renato Estrada Cáceres would like to thank the National Council for Scientific and Technological Development (Conselho Nacional de Desenvolvimento Científico e Tecnológico - CNPq) for the support provided through the doctoral scholarship (Proc. Nº: 142219/2017-7). Antonio D. de Figueiredo wishes to acknowledge the financial support of the National Council for Scientific and Technological Development - CNPq (Proc. Nº: 305055/2019-4). Renata Monte would also like to acknowledge the financial support of the National Council for Scientific and Technological Development – CNPq (Proc. N°: 437143/2018-0).

5. References

ARMELIN, H. Rebound and thoughening mechanisms in steel fibre reinforced dry-mix shotcrete. 1997. Thesis (PhD) - Canada, 1997.

ASSOCIAÇÃO BRASILEIRA NORMAS TÉCNICAS - ABNT. NBR 15530: fibras de aço para concreto – Requisitos e métodos de ensaio. Rio de Janeiro, 2019. 38 p. (In Portuguese).

AUSTIN, S. A.; PEASTON, P. H.; ROBINS, P. J. Material and fibre losses with fibre reinforced sprayed concrete. Construction and Building Materials, v. 11, p. 291-298, 1997.

BANTHIA, N.; TROTTIER, J.; BEAUPRÉ, D. Steel-fiber-reinforced wet-mix shotcrete: comparison with cast concrete. Journal of Materials in Civil Engineering, v. 6, n. 3, p. 430-437, 1994.

BENTUR, A.; MINDESS, S. Fibre Reinforced Cementitious Composites. 2nd ed., United Kingdom. Taylor & Francis, 2007.

BERNARD, E. S. Correlation in the behavior of fibre reinforced shotcrete beam and panel specimens. Materials and Strucutres, v. 35, p. 156-164, 2002.

BERNARD, E. S. Influence of Test Machine Control Method on Flexural Performance of Fiber Reinforced Concrete Beams. Journal of ASTM International, v. 6, n. 9, p. 1-16, 2009

BERNARD, E. S. Development of a 1200-mm-Diameter Round Panel Test for Post-Crack Assessment of Fiber-Reinforced Concrete. Advanced in Civil Engineering Materials, v. 2, n. 1, p. 457-471, 2013.

BERNARD, E. S.; THOMAS, A. H. Fibre reinforced sprayed concrete for ground support. Tunnelling and Underground Space Technology, v. 99, p. 103302, 2020.

BLANCO, A.; PUJADAS, P.; CAVALARO, S., de la FUENTE, A.; AGUADO, A. Constitutive model for fibre reinforced concrete based on the Barcelona test. Cement and Concrete Composites, v. 53, p. 327-340, 2014.

BORGES, L. A.; MONTE, R.; RAMBO, D. A. S.; FIGUEIREDO, A. D. Evaluation of post-cracking behavior of fiber reinforced concrete using indirect tension test. Construction & Building Materials, v. 204, p. 510-519, 2019.

577 CARMONA, S.; AGUADO, A.; MOLINS, C. Characterization of the properties of steel fiber reinforced
578 concrete by means of the generalized Barcelona test. Construction and Building Materials,
579 v. 48, p. 592-600, 2013.
580 CARMONA, S.; MOLINS, C.; AGUADO, A. Correlation between bending test and Barcelona tests to
581 determine FRC properties. Construction and Building Materials, v. 181, p. 673-686, 2018.
582 CARMONA, S.; MOLINS, C. Use of BCN test for controlling tension capacity of fiber reinforced
583 shotcrete in mining works. Construction and Building Materials, v. 198, p. 399-410, 2019.
584 CAVALARO, S. H. P.; AGUADO, A. Intrinsic scatter of FRC: an alternative philosophy to estimate
585 characteristic values. Materials and Structures, v. 48, n. 11, p. 3537–3555, 2015.
586 CAVALARO, S. H. P.; LÓPEZ, R.; TORRENTS, J. M.; AGUADO, A. Improved assessment of fibre content
587 and orientation with inductive method in SFRC. Materials and Structures, v. 48, pp. 1859-
588 1873, 2015.
589 CAVALARO, S. H. P.; LÓPEZ, R.; TORRENTS, J. M.; AGUADO, A.; GARCÍA, P. Assessment of fibre
590 content and 3D profile in cylindrical SFRC specimens. Materials and Structures, v. 49, p. 577-
591 595, 2016.
592 CNR. CNR-DT 204 /2006 Guide for the Design and Construction of Fiber-Reinforced Concrete
593 Structures, Italian National Research Council, Rome, 2006.
594 CPH. Instrucción del Hormigón Estructural EHE-08, Ministerio de Fomento, Madrid, 2008.
595 DI PRISCO, M.; LAMPERTI, M.; LAPOLLA, S. Double-edge wedge splitting test: preliminary results. In:
596 7th INTERNATIONAL CONFERENCE ON FRACTURE MECHANICS OF CONCRETE STRUCTURES
597 – FRAMCO-7 – PROCEEDINGS. Seowipo, Jeju (Korea): IA-FraMCoS, pp. 1579-1586, May 23 –
598 28, 2010.
599 DI PRISCO, M.; COLOMBO, M.; DOZIO, D. Fibre-reinforced concrete in fib Model Code 2010:
600 Principles, models and test validation. Structural Concrete, v. 14, n. 4, p. 342–361, 2013.
601 DI PRISCO, M.; FERRARA, L.; LAMPERTI, M. G. L. Double edge wedge splitting (DEWS): an indirect
602 tension test to identify post-cracking behavior of fibre reinforced cementitious composites.
603 Materials and Structures, v. 46, p. 1893-1918, 2013.
604 DUPONT, D. Modelling and experimental validation of the constitutive law (σ-Ɛ) and cracking
605 behavior of steel fibre reinforced concrete, PhD Thesis, Katholieke Universiteit Leuven,
606 2003.
607 EFNARC. European Specification for Sprayed Concrete. European Federation of Producers and
608 Applicators of Specialist Products for Structure (EFNARC), Hampshire, UK, 1996. 30p.
609 EN 14651. Test method for metallic fibre concrete – Measuring the flexural tensile strength (limit of
610 proportionality (LOP), residual), 2007.
611 EN 14488-3. Testing sprayed concrete – Part 3: Flexural strengths (first peak, ultimate and residual)
612 of fibre reinforced beam specimens. European Standard, 2004.
613 FIB, Model Code 2010, Vol 1 & 2. International Federation for Structural Concrete (fib), Lausanne,
614 Switzerland, 2010.
615 FIGUEIREDO, A. D. Parâmetros de controle e dosagem do concreto projetado com fibras de aço.
616 1997. Tese (Doutorado). Escola Politécnica, Universidade de São Paulo, São Paulo, 1997. (In
617 Portuguese).
618 FREUND, J. E.; SIMON, G. A. Estatística aplicada. Economia, administração e contabilidade. 9th ed.,
619 Porto Alegre: Bookman, 2002. (In Portuguese).
620 GALEOTE, E.; BLANCO, A.; CAVALARO, S. H.; de la FUENTE, A. Correlation between the Barcelona
621 test and the bending test in fibre reinforced concrete. Construction and Building Materials,
622 v. 152, p. 529 - 538, 2017.

GALOBARDES, I.; FIGUEIREDO, A. D. Correlation between beam and Barcelona tests for FRC quality control for structural application. Fibre Concrete 2015. September 10-11, Prague, Czech Republic, 2015.

GALOBARDES, I. ; SILVA, C. S. ; FIGUEIREDO, A. D.; CAVALARO, S. H. P.; GOODIER, C. I. Alternative control of steel fibre reinforced sprayed concrete (SFRSC). Construction and Building Materials, v. 223, p. 1008 – 1015, 2019.

GINOUSE, N.; JOLIN, M. Mechanism of placement in sprayed concrete. Tunnelling and Underground Space Technology, v. 58, p. 177 - 185, 2016.

ITA Working Group No. 12 and ITAtech, ITA Report No. 24, 2020. Permanent Sprayed Concrete Linings, October 2020. International Tunneling Association.

JOLIN, M. Mechanisms of placement and stability of dry process shotcrete. Thesis (PhD) – Department of civil engineering, The University of British Columbia. Vancouver, Canada, 1999.

JUHASZ, P. K.; NAGY, L.; SHACUL, P. Correlation of the results of the standard beam and EFNARC panel test. Proceeding of the World Tunnel Congress 2017 - Surface challenges - Underground solutions. Bergen, Norway, 2017.

KALIL, R. Z.; ESCARIZ, R. C.; FIGUEIREDO, A. D. Elaboração de método de ensaio para determinação do teor de fibras em concreto endurecido. In: CONGRESSO BRASILEIRO DO CONCRETO. 52., 2010, Fortaleza. Instituto Brasileiro do Concreto - IBRACON, 2010. (In Portuguese).

KAUFMANN, J.; FRECH, K.; SCHUETZ, F.; MÜNCH, B. Rebound and orientation of fibers in wet sprayed concrete applications. Construction and Building Materials, v. 49, p. 15-22, 2013.

LARIVE, C; BOUTEILLE, S.; BERTHOZ, N. ZAPELLI, S. Fiber-reinforced sprayed concrete as a permanent tunnel lining. Structural Engineering International, 2020.

LOK, T. S.; XIAO, J. R. Tensile behaviour and moment-curvature relationship of steel fibre reinforced concrete. Magazine of Concrete Research, v. 50, n. 4, p. 359–368, 1998.

MONTE, R.; de la FUENTE, A.; FIGUEIREDO, A. D.; AGUADO, A. Barcelona Test as an Alternative Method to Control and Design Fiber-Reinforced Concrete Pipes. ACI Structural Journal, v. 113, p. 1175-1184, 2016.

MONTEIRO, V.; SILVA, F. The use of the Barcelona test as quality control of fiber reinforced shotcrete for underground mining. Construction and Building Materials, v. 262, p. 120719, 2020.

MORGAN, D. R.; MINDESS, S.; CHEN, L. Testing and specifying toughness for fiber reinforced concrete and shotcrete. In: Second University-Industry Workshop on Fiber Reinforced Concrete and Other Advanced Materials. Toronto, Canada, 1995. Proceedings. P.29-50.

NGUYEN, T. Constitutive modelling of fibre reinforced concrete and shotcrete. 2003. 234p. Ph.D. Thesis – University of Tasmania.

NOGUEIRA, A. B.; SIMÃO, L. C. R.; MONTE, R.; SALVADOR, R. P.; FIGUEIREDO, A. D. Evaluation of the repeatability and reproductibility of the double punch test. Construction and Building Materials, 10p, 2020. https://doi.org/10.1016/j.conbuildmat.2020.121145

PUJADAS, P.; BLANCO, A.; CAVALARO, S. H. P.; de la FUENTE, A.; AGUADO, A. New analytical model to generalize the Barcelona test using axial displacement. Journal of Civil Engineering and Management, v. 19, n. 2, p. 259-271, 2013.

RAMBO, D. A. S.; BLANCO, A.; FIGUEIREDO, A. D.; SANTOS, E. R. F.; TOLEDO, R. D.; GOMES, O. F. M. Study of temperature effect on macro-synthetic fiber reinforced concretes by means of Barcelona tests: An approach focused on tunnels assessment. Construction and Building Materials, v. 158, p. 443-453, 2018.

ROBINS, P. J.; AUSTIN, S.; JONES; P. A. Spatial distribution of steel fibres in sprayed and cast concrete. Magazine of Concrete Research, v. 55, n. 3, p. 225-235, 2003.

SALUDES, S. R. Ensayo de doble puncionamiento aplicado al hormigón reforzado con fibras (Ensayo Barcelona). Minor Thesis, UPC, Barcelona, España, 2006. (In Spanish).

SEGURA-CASTILLO, L., CAVALARO, S.H.P., GOODIER, C., AGUADO, A., AUSTIN, S. Fibre distribution and tensile response anisotropy in sprayed fibre reinforced concrete. Mater Struct 51, 29 (2018). https://doi.org/10.1617/s11527-018-1156-5

SILVA, C. L. Proposta de metodologia alternativa para controle de qualidade da aplicação estrutural do concreto projetado reforçado com fibras de aço. 2017. Dissertação (Mestrado). Escola Politécnica, Universidade de São Paulo, São Paulo, 2017. (In Portuguese).

SIMÃO, L. C. R.; NOGUEIRA, A. B.; MONTE, R.; SALVADOR, R. P.; FIGUEIREDO, A. D. Influence of the instability of the double punch test on the post-crack response of fiber-reinforced concrete. Construction and Building Materials, v. 217, p. 185-192, 2019.

THAI, D. K.; NGUYEN, D. L.; NGUYEN, D. D. A calibration of the material model for FRC. Construction and Building Materials, v. 254, p. 119293, 2020.

TLEMAT, H.; PILAKOUTAS, K.; NEOCLEOUS, K. Modelling of SFRC using inverse finite element analysis. Materials and Structures/Materiaux et Constructions, v. 39, n. 2, p. 221–233, 2006.

TORRENTS, J. M.; BLANCO, A.; PUJADAS, P.; AGUADO, A.; JUAN-GARCÍA, P.; SÁNCHEZ-MORAGUES, M. A. Inductive method for assessing the amount and orientation of steel fibers in concrete. Materials and Structures, v. 45, n. 10, pp. 1577–1592, 24 Abr. 2012.

TRAN, V. N. G.; BERNARD, E. S.; BEASLEY, A. J. Constitutive Modeling of Fiber Reinforced Shotcrete Panels. Journal of Engineering Mechanic, v. 131 (5), p. 512-521, 2005.

VANDEWALLE, L. *et al*. RECOMMENDATION, F. RILEM TC 162-TDF: “Test and design methods for steel fibre reinforced concrete” σ-ε-design method. Materials and Structures/Materiaux et Constructions, v. 36, n. 262, p. 560–567, 2003.